Journal of Molecular Liquids 347 (2022) 117990

Contents lists available at ScienceDirect

Journal of Molecular Liquids

journal homepage: www.elsevier.com/locate/molliq

Adsorption of atrazine herbicide from water by diospyros kaki fruit waste activated carbon

Yamil L. Salomón [a], Jordana Georgin [a], Dison S.P. Franco [b], Matias S. Netto [b], Daniel G.A. Piccilli [a], Edson Luiz Foletto [b], Diana Pinto [c], Marcos L.S. Oliveira [c,d], Guilherme L. Dotto [b,*]

[a] Sanitary and Environmental Engineering Department, Federal University of Santa Maria, Santa Maria 97105–900, Brazil
[b] Chemical Engineering Department, Federal University of Santa Maria, Santa Maria 97105–900, Brazil
[c] Department of Civil and Environmental Engineering, Universidad de la Costa, Barranquilla, Colombia
[d] Universidad de Lima, Avenida Javier Prado Este 4600, Santiago de Surco 1503, Peru

ARTICLE INFO

Article history:
Received 27 July 2021
Revised 5 October 2021
Accepted 27 October 2021
Available online 10 November 2021

Keywords:
Diospyros kaki
Adsorption
Atrazine
Isotherms
Thermodynamics

ABSTRACT

In this work, *Diospyros kaki* fruit waste was employed as a precursor material to develop a high surface area activated carbon, which efficiently removed the toxic herbicide atrazine (ATZ) from synthetic water solutions and river waters. The alternative activated carbon presented excellent characteristics and structure, including high values of specific surface area (1067 $m^2\ g^{-1}$) and pore volume (0.530 $cm^3\ g^{-1}$) and some important functional groups on the surface. The temperature positively influenced the adsorption capacity, from 194.20 to 211.51 mg g^{-1}. The Freundlich model was the proper one to represent the equilibrium data. Thermodynamic parameters confirmed the endothermic nature of the adsorption process. Kinetic studies confirmed that equilibrium was reached until 240 min, regardless of ATZ initial concentration. The LDF model adjusted well to the kinetic data, resulting in a diffusion coefficient ranging from $0.89x10^{-9}$ to $1.63x10^{-9}$ $cm^2\ s^{-1}$ as the ATZ concentration increased. The activated carbon also decreased 85% of the ATZ concentration in a river water sample. Overall, the activated carbon developed from *Diospyros kaki* fruit waste presented an efficient ATZ removal from aqueous matrices.

1. Introduction

In recent years, the agricultural sectors have grown exponentially, intensified by the high degree of management employed in the crops. In this sense, the effective control of weeds becomes essential, but weeds are increasingly resistant, requiring higher concentrations of pesticides. Atrazine (ATZ) is an herbicide of the class of triazines, widely used in corn and sugar cane crops, being extensively spread worldwide due to its high effectiveness in combating weeds [1]. However, due to low biodegradability and high persistence in soil and sediments, atrazine easily contaminates the surface and groundwater [2,3]. The major concern relating to the ATZ is health damage since it affects the endocrine and nervous system and is also related to breast cancer [4]. The ATZ also affects the aquatic and terrestrial biota causing problems in frogs, fish, and other wild animals [5]. As a result, atrazine in many European countries is prohibited [6]. However, it is still allowed in Brazil and the United States, where the maximum allowed value of Atrazine in water is 2 μg L^{-1} and 3 μg L^{-1}, respectively [7].

Several techniques proposing the removal of ATZ from aqueous solutions are described in the literature, highlighting adsorption, with the advantage of using low-cost residues as adsorbents and easy operational design [8–12]. Agroindustrial residues are widely applied in adsorption studies because they have a negligible cost of obtaining them. However, most of them have a low surface area, which leads to unsatisfactory removal values [13,14]. Carbonization is one of the techniques applied since it alters the structural properties of materials, increasing the surface area [15–17]. In this sense, in the study by Wei and collaborators [18], activated carbon samples were produced from apricot, walnut, and wood residues to remove chromium (Cr) and ATZ. Gao [4] prepared biochars from sawdust and corn husks for improved ATZ removal. Tchikuala [19] developed activated carbon from the natural fibers of baobab residues to remove the herbicide Diuron. Salomón [20] obtained a high removal performance of the herbicide 2,4-dichlorophenoxyacetic acid (2,4-D) in water using activated carbon derived from the endocarp of the Queen palm (*Syagrus romanzoffiana*). Binh and Nguyen [21] used corn cob to produce an alternative activated carbon employed in the herbicide 2,4-D adsorption.

The edible fruits of the *Diospyros kaki* (persimmon) tree are widely consumed in Latin America and Asian countries, including

* Corresponding author.
E-mail address: guilherme.dotto@ufsm.br (G.L. Dotto).

https://doi.org/10.1016/j.molliq.2021.117990
0167-7322/

Japan, China, and Korea. It belongs to the Ebenaceae family, has high nutritional value, and is used in several dishes [22,23]. The fruit pulp is rich in starch, pectin, sugars, with a very high vitamin A and low acid content. Thus this fruit moves a large sector of the agribusiness[24–26]. In addition, the fruits have large and sweet berry shapes, whose color varies from yellow to red; inside are the seeds, which are not consumed becoming waste. In this way, the seeds can be converted into an activated carbon through carbonization and activation, adding value to this waste material.

This work aims to convert *Diospyros kaki* seeds to high surface area activated carbon for removing atrazine (ATZ) from synthetic solutions and river waters. Different techniques were employed to characterize in detail the new adsorbent material. Furthermore, concerning the study with synthetic solutions, thermodynamic, kinetic, and equilibrium isotherm evaluations of atrazine adsorption on the activated carbon were developed. Finally, the application of this new adsorbent in real river water samples aimed to reduce ATZ concentration until the desirable standards of Brazil legislation for waters.

2. Material and methods

2.1. Chemicals

The chemical compounds zinc chloride ($ZnCl_2$), hydrochloric acid (HCl), and atrazine (chemical formula: $C_8H_{14}ClN_5$; molecular weight: 215.69 g mol^{-1}; molar volume: 169.8 cm^3 mol^{-1}) were all acquired with an analytical degree from Sigma-Aldrich. The stock solution was prepared by accurately dissolving the 1 g L^{-1} of atrazine in methanol (10 % V/V) since atrazine has low water solubility in this concentration. The diluted solutions were further diluted until reaching the desired concentration. All the water employed for the preparation of the solutions was previously deionized.

2.2. Preparation of activated carbon from Diospyros kaki seeds

The *Diospyros kaki* fruits were obtained commercially in the south of Brazil, being that their seeds were separated and washed with distilled water. Then, the seeds were dried and crushed in a knife mill to pass through a 250 μm sieve, obtaining the precursor material called Persimmon seed residue (PSR). Preliminarily, the material was placed in contact with a NaOH solution (2.5 mol L^{-1}) for 2 h, being the mixture posteriorly washed several times until reaching neutral pH (7). This step was performed to remove the natural oils present in the vegetable material.

The preparation of activated carbon was carried out using 10 g of PSR and 10 g of zinc chloride ($ZnCl_2$). First, PSR and $ZnCl_2$ were mixed with distilled water until obtaining a homogeneous dark-colored mass. Next, the mass was taken to an oven and dried at a temperature of 378 K for 48 h, being posteriorly crushed until particles with a diameter below 355 μm. Then, pyrolysis was performed using a quartz tube under N_2 atmosphere at a flow rate of 0.25 L min^{-1} and heating rate of 10 °C min^{-1} until the temperature reached 650 °C, maintained for 80 min at this temperature. After this, the material was placed in contact with an HCl solution (10 mol L^{-1}) for 120 min under stirring to solubilize and extract the $ZnCl_2$ present on the sample. In sequence, the solid particles were washed with distilled water several times until they reached neutrality (pH = 7), separated by decantation, and taken to the oven at 100 °C for 24 h. After drying, the sample was comminuted and sieved to obtain particles with a diameter below 149 μm and entitled Persimmon seed activated carbon (PSAC). The estimated percentage yield of activated carbon (Y, %) was obtained from the initial mass (m_0, g) and final mass (m_f, g), as presented by Eq. (1):

$$Y\ ,\ \%\ = \left(1 - \frac{m_f}{m_0}\right) 100 \quad (1)$$

2.3. Characterization techniques

Different techniques were used to characterize the precursor material (PSR) and activated carbon (PSAC) samples, as follows: the specific surface area (S_{BET}, m^2 g^{-1}) was obtained by the adsorption/desorption isotherms of N_2 through ASAP 2020. The total pore volume (V_T, cm^3 g^{-1}) was determined considering the amount of N_2 adsorbed on the material surface at a relative pressure (P/P_0) of 0.99. Before and after the pyrolysis step, the surface images were observed using a scanning electron microscope (SEM) at 10 kV (Vega 3 SB, Tescan, Czech Republic). The same equipment was used to obtain EDS analysis (Energy-dispersive X-ray spectroscopy). The materials' Fourier transform infrared spectra (FT-IR) were obtained using an IR-Prestige-21 (Shimadzu, Japan) spectrometer, with a spectral range from 4500 to 500 cm^{-1}. X-ray diffraction (XRD) was used to identify crystallographic structures with a computer-controlled X-ray diffractometer (Miniflex 300, Rigaku, Japan). Thermogravimetric analysis was performed using 10 mg of material on a thermogravimetric analyzer (STA 449 F3 Jupiter, Netzsch, Germany) under oxidizing atmosphere (synthetic air) with a volumetric flow rate of 100 mL min^{-1}. The crucible used was alumina. A heating rate of 10 K min^{-1} from room temperature to 1073.15 K was used.

2.4. ATZ adsorption experiments

The atrazine herbicide (ATZ) adsorption tests onto the PSAC sample were performed on a thermostatic stirrer (MA093, Marconi, Brazil) at 150 rpm. The ATZ concentration in the liquid phase was measured on the spectrophotometer (UV mini 1240, Shimadzu) at a maximum wavelength of 222 nm. After each experiment, the suspensions were centrifuged at 4000 rpm for 20 min to perform a solid–liquid separation. All experiments were carried out at the natural pH of the solution (pH = 6.5) using 25 mL of liquid solution. The optimum adsorbent dosage was provided using Erlenmeyer flasks, at the concentration of 50 mg L^{-1} of ATZ, being that in each flask, 0.2, 0.4, 0.6, 0.8, and 1 g L^{-1} of PSAC was added and then shaken at 298 K for 180 min. After that, the isotherms experiments were performed at 298, 308, 318, and 328 K with the initial ATZ concentration ranging from 0 to 150 mg L^{-1}. Finally, kinetic studies were performed for the initial ATZ concentration of 25, 50, and 100 mg L^{-1}, where the liquid samples were collected at 0, 5, 10, 20, 30, 60, 120, 180, and 240 min. The equations employed to calculate the adsorption capacity at any time (q_t, mg g^{-1}), adsorption capacity at the equilibrium (q_e, mg g^{-1}), and removal percentage (R, %) are shown in Supplementary material (**S1**).

2.5. Isotherms, thermodynamics, and kinetics

For the adsorption equilibrium study, the following models were chosen: Freundlich [27], Dubinin-Radushkevich [28], Temkin [29], and Langmuir [30]. Concerning the calculation of thermodynamic parameters, it was employed the approach suggested elsewhere [31]. The linear driving force model (LDF) [32] was chosen to fit the experimental kinetic data. The respective models and equations are exhibited in Supplementary material (**S2** to **S4**).

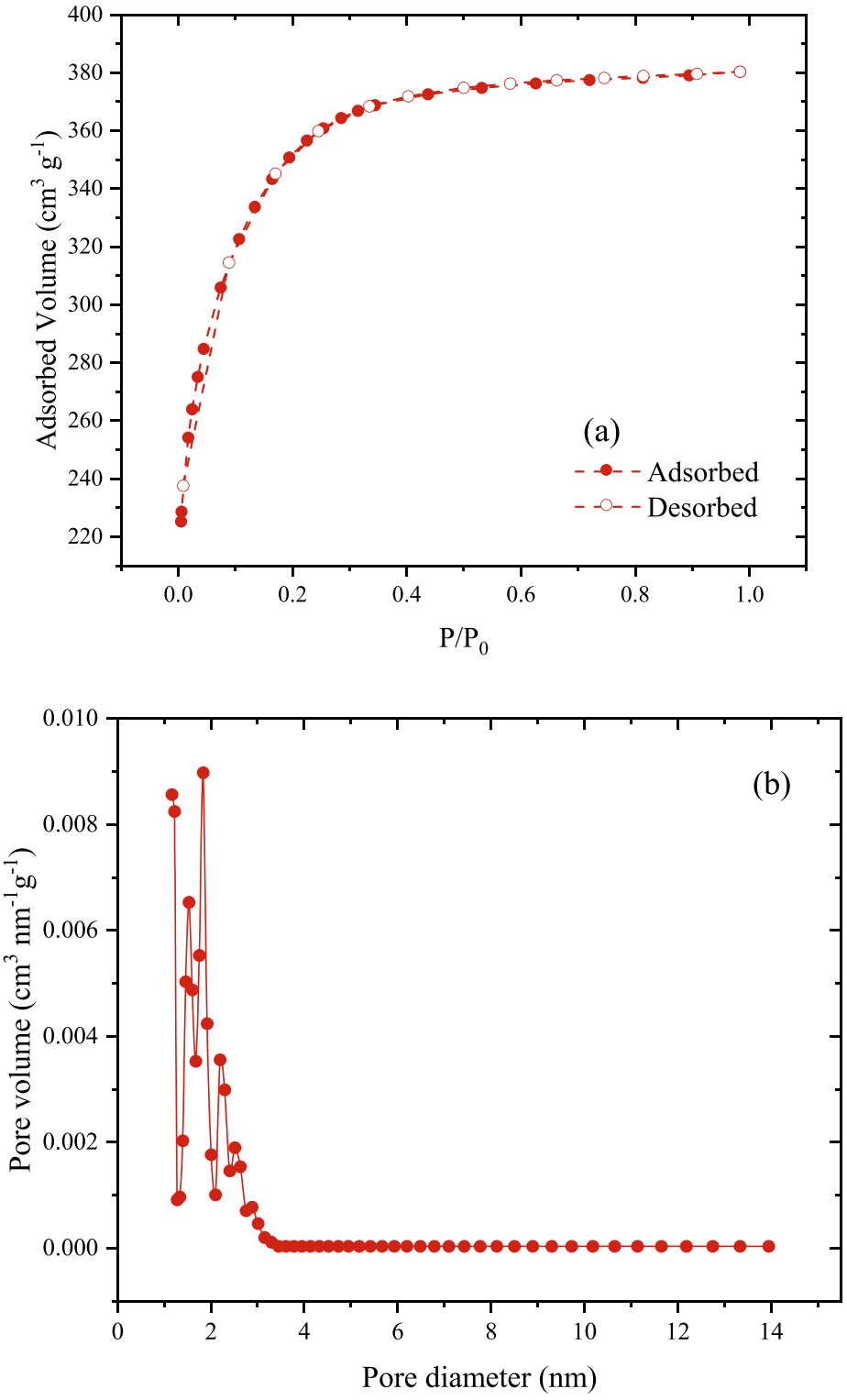

Fig. 1. (a) N_2 adsorption–desorption isotherms and (b) desorption pore size distribution for PSAC sample.

2.6. Parameter estimation and evaluation

Concerning the LDF model, the parameter was estimated using *lsqnonlin,* and the solution of the model was done by employing the ode15s. The parameters for each chosen model for equilibrium curves were estimated using the Matlab software with build-in functions: *particleswarm*, *nlinfit*, *lsqnonlin*. Finally, the quality of each model was evaluated through statistical parameters: determination coefficient (R^2), adjusted determination coefficient (R^2_{adj}), average relative error (*ARE*, %), and mean square error (*MSR*, (mg $g^{-1})^2$). The respective equations are presented in the supplementary material (**S5**).

2.7. Treatment of river water containing ATZ

It is important to highlight that real waters containing ATZ (river waters, for example) have different characteristics than synthetic solutions. The main aspects are related to different salts,

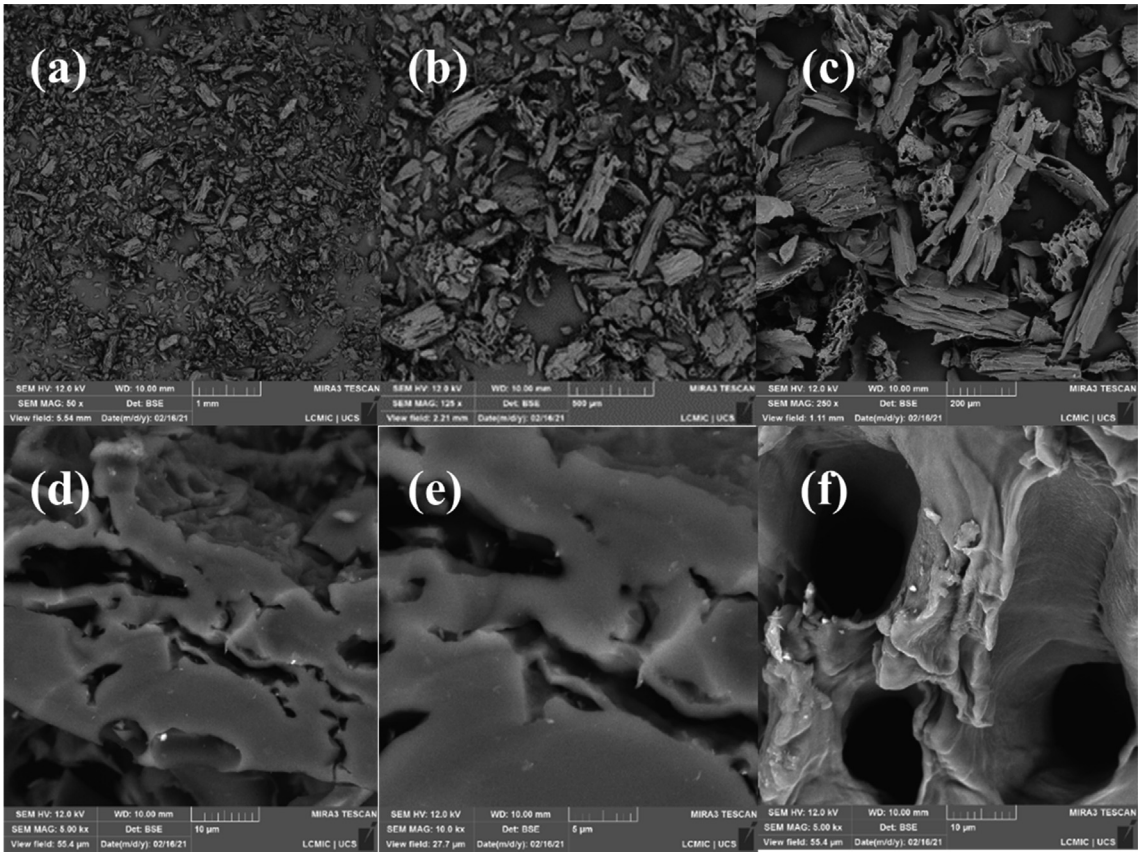

Fig. 2. SEM images of (a, b, c) PSR sample and (d, e, f) PSAC sample under different magnifications.

metals, organic compounds, and other organic molecules. The presence of these compounds directly affects the adsorption capacity since the compounds can compete for the available activated sites or interfere in the solubility of the ATZ, causing it not to be adsorbed at all. However, these effects are not present or are mitigated when studying the adsorption experiment using an ideal solution. Furthermore, the performance of an adsorbent to uptake ATZ can be evaluated in synthetic solutions with concentrations in the range of mg L^{-1} [8].

On the contrary, the ATZ concentrations in real water samples like river waters range from ng L^{-1} to μg L^{-1} [7]. Adsorption experiments in river water were carried out to check the efficiency of activated carbon developed in this work in real samples (PSAC). A sample of 100 mL from the Jacuí river (Agudo city, Brazil; 29°38′42 "S – 53°14′24″ W) was collected. First, the river water sample was filtered with the intuition of removing any coarse dirt. After that, atrazine was quantified by HPLC. For this was employed a liquid chromatographer system (1100 Series, Agilent Technologies, Japan) equipped with a binary pump (G1312A, Agilent Technologies), a vacuum degasser (G1379A, Agilent Technologies), and an auto-sampler (G1313A, Agilent Technologies) with 100 positions for 2 mL vessels (PTFE/silicon septum, Clear vial, Agilent Technologies) coupled with inductively coupled plasma triple quadrupole mass spectrometer (8800 ICP-QQQ, Agilent Technologies). It was found that the initial atrazine concentration was 4.7 μg L^{-1}. Then, duplicate adsorption experiments were carried out with adsorbadsorbent dosage of 3 g L^{-1} at the natural pH of the river water (6 ∼ 7). The suspension was stirred at 150 rpm for 2 h and posteriorly separated by centrifugation. ATZ concentration after adsorption was quantified by HPLC.

3. Results and discussion

3.1. PSAC characterization results

Fig. 1 shows the N_2 adsorption/desorption isotherms and pore size distribution for the activated carbon sample. According to IUPAC, it was classified as type I, characteristic of microporous material with pore diameter ranging from 1.0 to 3.5 nm, resulting in an average pore diameter of 1.84 nm [33]. In addition, the specific surface area (S_{BET}) was 1067 m^2 $g^{-1,}$ and the total pore volume (V_p) was 0.530 cm^3 g^{-1}. As highlighted below, these findings follow other published works using different vegetable biomasses as precursor materials for preparing activated carbons. For example, Lima et al. [34] obtained a surface area of 1457 m^2 g^{-1} and V_p of 0.666 cm^3 g^{-1} using nutshell as precursor biomass, while Kasperiski [35] obtained a surface area of 1469 m^2 g^{-1} and pore volume of 0.401 cm^3 g^{-1} using *Caesalpinia ferrea* waste. In addition, Leite et al. [36] used the avocado seed to prepare activated carbon samples, obtaining specific surface area values ranging from 1122 to1587 m^2 g^{-1} and pore volume values ranging from 0.600 to 0.084 cm^3 g^{-1}.

Fig. 2 (a), (b), and (c) corresponds to SEM images for the PSR sample. Particles with heterogeneous shapes form the material surface but with a smooth surface with irregularities or cavities. This type of structure has also been observed on other materials of vegetable origin [14,37,38]. In addition, morphological changes have occurred after the pyrolysis process (Fig. 2 d, e, f), appearing in new cavities and cracks. These changes are also evident in other activated carbon samples derived from vegetable wastes [39–41]. These new spaces can favor the adsorption since they become occupied by the adsorbate molecules.

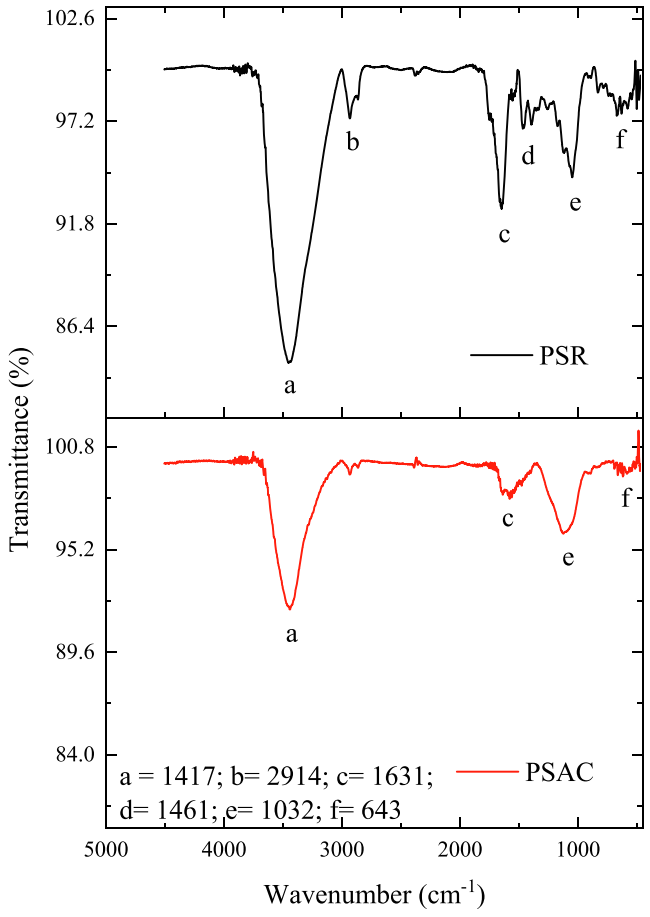

Fig. 3. FT-IR spectra of PSR and PSAC samples.

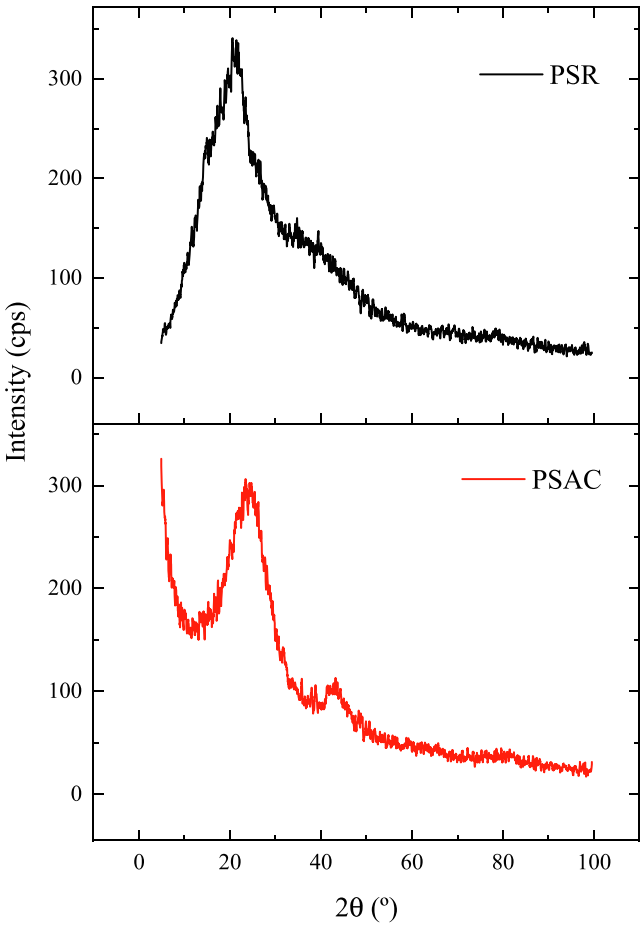

Fig. 4. XRD of PSR and PSAC samples.

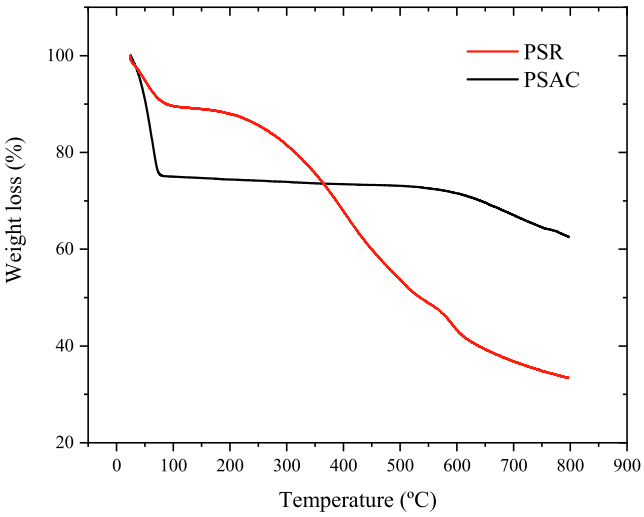

Fig. 5. Thermogravimetric analysis and for the PSR and PSAC samples.

Fig. 3 shows the FT-IR spectra of PSR and PSAC samples. It is noted that a large part of the bands will remain in the material after the pyrolysis step; however, they have lost their intensity. The remained bands after the carbonization/activation step were: (a), which corresponds to the OH stretching [42], the (c) identified as the CO stretching [43]. After that, it is possible to identify the CO, C = C, and CCO stretching vibration (e). These groups are related to cellulose, hemicellulose, and lignin [44]. The last remaining band (f) is related to the C-H aliphatic and aromatic bonds [45]. The bands that disappear after pyrolysis can be identified as the C-H (b) bond [43] and to stretching vibrations C-O, C-H, or C-C (d) [46]. This trend indicates that the lignin and hemicellulose content diminishes in the process, generating C = C bonds on the material. Similar results for removing groups disposed on the surface of plant residues by chemical or physical processes have been reported elsewhere [47,48]. However, certain defined groups on the activated carbon surface are favorable for adsorption [49].

Fig. 4 exhibits the diffraction patterns of both materials. Both samples presented broad, amorphous peaks related to the amorphous carbon at 22.1 ° for the PSR and 21.5 for the PSAC. After the carbonization and activation step, it was found that the material presents a lower peak at 45°; this peak is related to the presence of carbon graphite [50]. In general, it is possible to mention that materials with disorganized structures may be favorable for the adsorption phenomena since they may present more space that favors the adsorption overall.

TGA (Fig. 5) curves make it possible to check the thermal stability and the decomposition profile of PSR and PSAC samples. The thermogravimetric profiles show that the PSR sample has three stages of decomposition, where the first stage corresponds to mass loss due to adsorbed water (between 50 °C and 100 °C) [51]. The second stage occurs above 250 °C, attributed to the decomposition of hemicellulose and cellulose [52]. The third, above 650 °C, refers to the decomposition of the carbonaceous skeleton [53,54]. On the other hand, the PSAC sample presented two stages of decomposition, being the first referring to water loss (around 100 °C) and the second stage (above 650 °C) referring to mass loss due to the

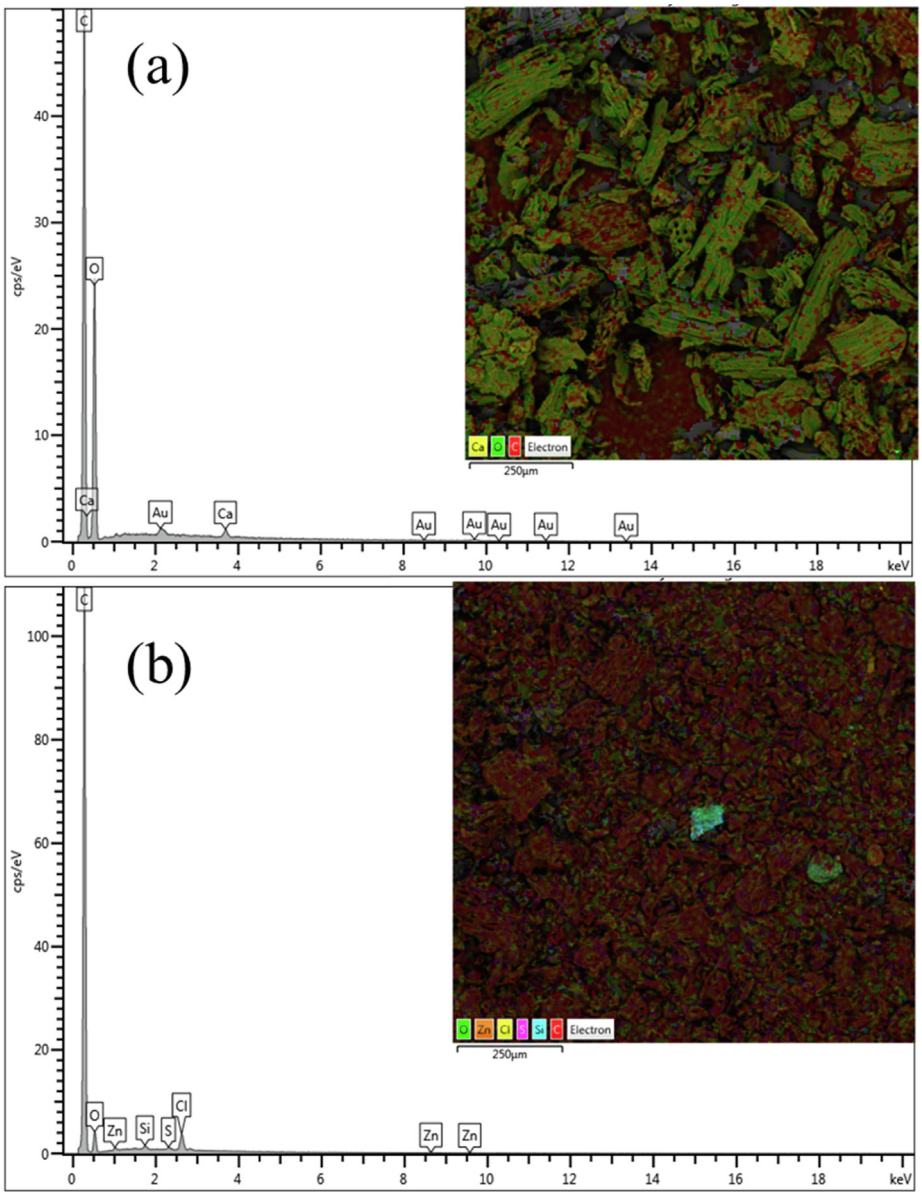

Fig. 6. EDS results for (a) PSR and (b) PSAC samples.

decomposition of lignin and carbonaceous skeleton [52,54]. Therefore, the thermal stability of the produced activated carbon (PSAC) can be ensured between 100 and 650 °C, where a constant value for the mass loss is observed.

The EDS results of PSR and PSAC samples are shown in Fig. 6. The main differences are in the amounts of carbon (red) and oxygen (green) present before and after the carbonization step. The PSR sample (Fig. 6a) contains higher oxygen and lower carbon content than the PSAC sample. In numerical values, the C content is 90 % for PSAC and 60% for PSR, thus confirming the preparation of a carbon-based adsorbent. This behavior occurred because, during the pyrolysis process, the volatile materials containing O are removed from the precursor, leading to a material with a high C percentage. Besides, based on the O/C molar ratio, which can be used to express an adsorbent's hydrophilic nature [55], the carbonaceous material can be seen to present greater aromaticity when compared to its precursor. These findings follow other studies that used materials of vegetable origin to obtain activated carbon [55–57].

3.2. Effect of PSAC dosage on ATZ adsorption

The effect of PSAC dosage on the herbicide adsorption capacity and efficiency is shown in Fig. 7a. The increase in the dosage causes inverse effects. The first one is the increase of the percentage removal, which goes from 48.09 to 97.88 %. The second is the adsorbent capacity that decreases from 120.96 to 49.23 mg g^{-1}. These behaviors are related to the number of available sites for the ATZ to be adsorbed. Considering that as the adsorbent dosage increases, the overall number of responsible sites increases as well. Besides that, the dosage effect also indicates the optimum dosage for the system, where the points cross each other. In this case, it was found that the dosage at 0.43 g L^{-1} leads to a removal of 77 % and an adsorption capacity of 91 mg g^{-1}.

3.3. ATZ equilibrium isotherms and adsorption thermodynamics

Isotherms were used to describe the relation of ATZ adsorption capacity (q_e) in PSAC, ranging the concentration (0–150 mg L^{-1}) and

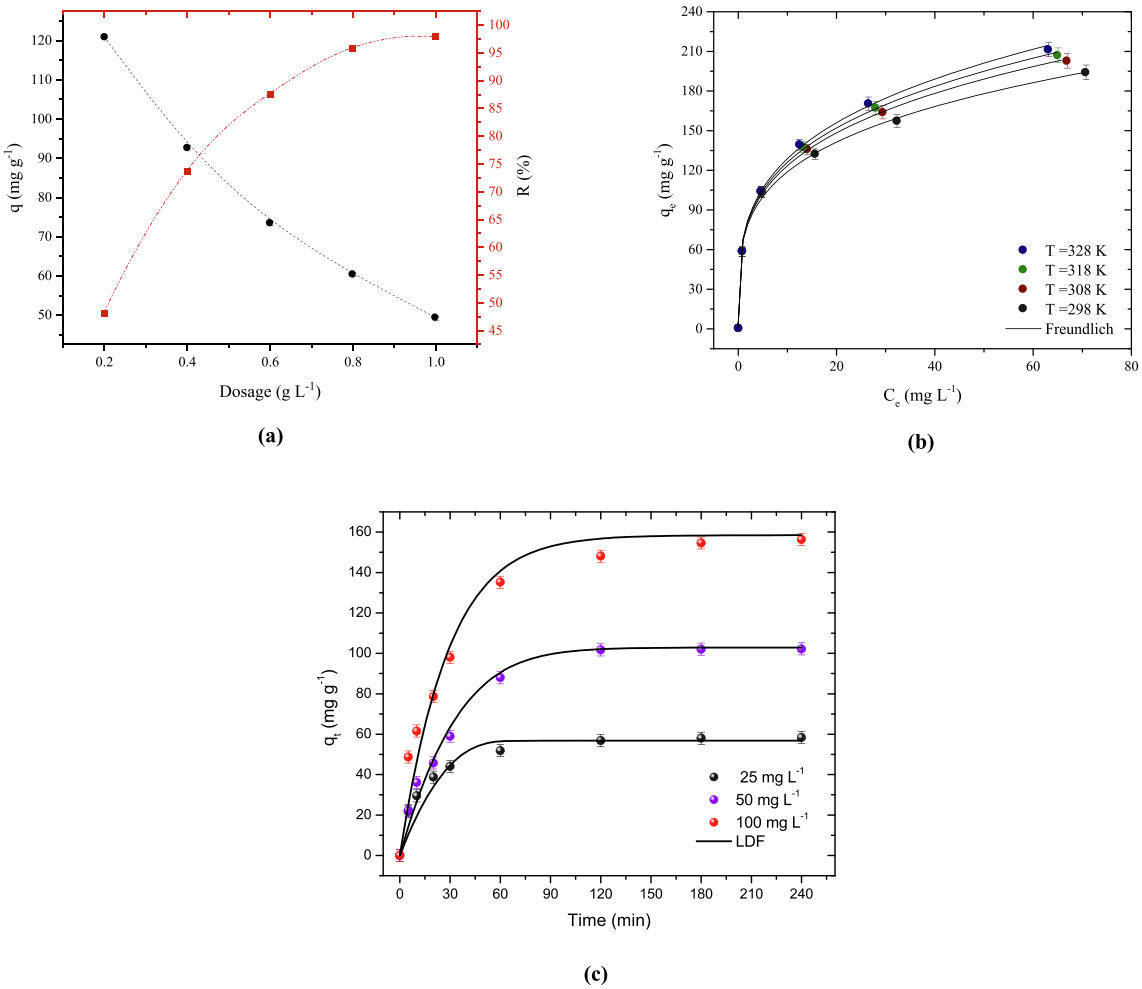

Fig. 7. ATZ adsorption results: (a) adsorbent dosage effect (C_0 = 50 mg L^{-1}, T = 298 K, t = 180 min, V = 25 mL, pH = 7.0); (b) isotherm curves (pH = 6.5, Adsorbent dosage = 0.43 g L^{-1}, V = 25 mL); (c) kinetic curves (pH = 6.5, Adsorbent dosage = 0.43 g L^{-1}, V = 25 mL).

temperature (298–328 K), as shown in Fig. 7b. The ATZ adsorption was favored by the increase in temperature (from 298 to 328 K); however, the adsorption capacity was only 8.9 %, from 194.20 to 211.51 mg g^{-1}, for an initial concentration of 150 mg L^{-1}. This increase may be related to an improvement in the process of mass transfer of ATZ molecules through the boundary layer with the increase in the temperature of the solution due to the reduction in water viscosity and the increase in solute mobility, corresponding to the increase in the temperature of the solution [58,59]. Similar behavior was also found by Alahabadi and Moussavi [60], using activated carbon prepared from the dry stem of *Calligonum comosum*. The capacity was from 348 to 748 mg g^{-1} when the temperature was raised from 283 to 313 K. It was also observed that the equilibrium curves were favorable since they were convex and presented high adsorption capacity coupled with high removal percentages. The plateau was not observed in the equilibrium curves. This trend indicates that PSAC has more adsorption sites to be occupied by ATZ, and consequently, the adsorbent can be used in higher concentrations than the used in this work.

From the experimental data, the parameters of four isotherm models were selected (Table 1). It was observed that the Freundlich model obtained a better fit compared to the other models. Freundlich model presented high values of determination coefficient (R^2 > 0.9983) and adjusted determination coefficient (R^2_{adj} > 0.9972) and lower values of *ARE* (<2.71 %) and *MSE* (<11.03 mg g^{-1}). The high value of the determination coefficient may suggest that the high heterogeneity plus the number of pores present on the surface of the adsorbent were fundamental for the ATZ adsorption, where different sites with various adsorption energies were performed. In addition, the value of $1/n$ < 1 indicates a favorable ATZ adsorption on the PSAC sample. The K_F value slightly increased with the temperature, indicating a better ATZ adsorption at 328 K. The results found for the Freundlich fit follow other reported works studying carbonaceous materials as adsorbents [61–66].

Table 2 was elaborated to verify the adsorption capacity of several adsorbents employed to remove ATZ in water. Among all the adsorbents analyzed, the activated carbon developed in this work presented the second-best adsorption capacity (q_{max} = 211.5 mg g^{-1}), indicating that the adsorbent is highly effective in removing ATZ in water.

The obtained thermodynamic parameters (Table 3) are in agreement with the isotherm results. The plot $\ln(K_e)$ *versus* $1/T$ presented a linear relation with an R^2 of 0.93. The system presented spontaneous ΔG^0 values from −18.00 to −20.74 kJ mol^{-1}, confirming that ATZ adsorption was favored at 328 K (more negative ΔG^0 values). The ΔS^0 value was 0.09 kJ mol^{-1} K^{-1}, being that the positive sign points out that some rearrangements on the adsorbent surface may have occurred during herbicide adsorption. The ΔH^0 value of 8.89 kJ mol^{-1} confirms that the ATZ adsorption on the activated

Table 1
Isotherm parameters for ATZ adsorption onto PSAC sample.

Temperature (K) Model	298	308	318	328
Langmuir				
q_L (mg g^{-1})	180.70	194.18	201.37	208.78
K_L (L mg^{-1})	0.3137	0.2622	0.2426	0.2266
R^2	0.9444	0.9493	0.9526	0.9563
R^2_{adj}	0.9073	0.9155	0.9210	0.9271
ARE (%)	14.63	14.69	14.55	14.31
MSE (mg g^{-1})^2	341.76	341.86	334.70	322.81
Freundlich				
K_F ((mg g^{-1})(mg L^{-1})$^{-1/nF}$)	66.01	66.52	66.92	67.44
$1/n$ (dimensionless)	0.2530	0.2666	0.2729	0.2789
R^2	0.9983	0.9990	0.9989	0.9985
R^2_{adj}	0.9972	0.9983	0.9981	0.9975
ARE (%)	2.50	2.25	2.46	2.71
MSE (mg g^{-1})^2	10.33	7.07	7.87	11.03
Dubinin-Radushkevich				
q_{mDR} (mg g^{-1})	150.07	155.45	158.19	160.96
βx10^7 (kJ^2 mol^{-1})	2.5421	2.5039	2.4110	2.3279
R^2	0.8443	0.8319	0.8263	0.8209
R^2_{adj}	0.7405	0.7199	0.7104	0.7016
ARE (%)	17.51	19.08	19.87	20.67
MSE (mg g^{-1})^2	957.01	1133.65	1226.34	1321.60
Temkin				
a (mg g^{-1})	85.09	80.67	79.85	79.00
b (L mg^{-1})	7.8949	6.5414	6.0132	5.5612
R^2	0.9798	0.9810	0.9815	0.9818
R^2_{adj}	0.6886	0.6639	0.6525	0.6419
ARE (%)	4.23	4.73	4.95	5.15
MSE (mg g^{-1})^2	53.91	58.14	60.55	63.25

Table 2
Maximum adsorption capacities of several adsorbents for the herbicide ATZ.

Adsorbent	pH (-)	T (K)	C_0 (mg L^{-1})	q_m (mg g^{-1})	Reference
Persimmon seed activated carbon	7	328	0–150	211.5	This work
Mixed biochars generated from corn straw and sawdust	–	298	15–55	48.6	[4]
Acid-activated zeolite-rich tufts	3.7	298	5–25	1.1	[9]
Sludge activated carbon	4	298	20–80	45.5	[67]
Alluvial soil	7	288	5–20	15.9	[68]
Rice soil	7	288	5–20	5.58	
Laterite	7	288	5–20	9.51	
ACs derived from apricot peel	3	293	60–100	46.3	[18]
Activated carbon modified with $C_{16}H_{26}SO_3$	2	308	70–110	222.22	[69]
Reduced graphene oxide supported by biochar	6	298	10	67.55	[70]
Magnetic carbon nanotubes	6	298	1–20	40.16	[66]
Multi-walled carbon nanotubes	6	298	4.2	17.35	[71]
Corn straw biochar	7	313	5–25	53.85	[72]
Bentonite modified with benzyl chloride octadecyl dimethyl ammonium	7	298	10–20	4.24	[73]
Iron-modified biochar	7	318	5–30	58.87	[74]

carbon is an endothermic process, in which predominantly physical forces act in the process (Van der Waals forces, < 20 kJ mol^{-1}) [75].

3.4. ATZ adsorption kinetics and application of the LDF model

Fig. 7c illustrates the time required for the ATZ/PSAC system to come into equilibrium. For these studies, three different herbicide concentrations were used, is found that the initial concentration little influenced the equilibrium time. The adsorption capacity

Table 3
Thermodynamics properties for ATZ adsorption onto PSAC sample.

T (K)	K_e (-)	ΔG^0 (kJ mol^{-1})	ΔH^0 (kJ mol^{-1})	ΔS^0 (kJ mol^{-1} K^{-1})
298.15	1425.0	−18.00	8.89	0.09
308.15	1538.3	−18.80		
318.15	1669.8	−19.62		
328.15	2001.2	−20.74		

Table 4
Kinetic parameters for ATZ adsorption onto PSAC sample.

LDFM	Initial ATZ concentration (mg L^{-1}) 25	50	100
q_{exp} (mg g^{-1})	58.31	102.16	156.38
q_{pred} (mg g^{-1})	56.86	102.85	158.46
k_{LDF} x10^4 (s^{-1})	0.0147	0.0169	0.0268
D_S x10^9 (cm^2 s^{-1})	0.89	1.02	1.63
R^2	0.9105	0.9842	0.9618
ARE (%)	23.95	13.56	17.62
MSE (mg g^{-1})^2	35.16	23.38	115.91

increased, reaching 58.03, 102.06, and 156.38 mg g^{-1} for the initial concentrations of 50, 100, and 200 mg L^{-1}, respectively. The experimental data show that the adsorption is rapid in the first minutes, related to the high quantity of available sites. After that, however, the adsorption sites have been progressively occupied over time, becoming saturated, decreasing the adsorption capacity [76]. Alahabadi and Moussavi [60] reported similar kinetic behavior when studying the adsorption of atrazine onto the *Calligonum Comosum* biochar. The linear driving force model (LDF) was fitted to the experimental data (Table 4) to interpret the kinetic results better. It can be observed through the statistical parameters that the model presented a satisfactory statistical adjustment ($R^2 \geq 0.9105$) and (*MSE* $\leq$ 115.91 (mg g^{-1})^2, and the values of adsorption capacity agree with those studied experimentally. In addition, the mass transfer coefficient (K_{LDF}) increased with the initial ATZ concentration, agreeing with the study reported by Zurro [77]. Last, the diffusion coefficient was estimated to be 0.89x10^{-9} to 1.63x10^{-9} cm^2 s^{-1}. Similar behavior was also reported by Moreno-Pérez [78] when studying the ketoprofen adsorption onto ZnAl/biochar.

In summary, the kinetic profiles revealed a fast ATZ adsorption. The majority of the phenomena occurred until 60 min. After the adsorption rate decreased, the equilibrium was attained at around 240 min. The LDF is close to the experimental data and can explain the curves and the trends concerning the ATZ concentration, adsorption capacity, and time.

3.5. Physical statistics modeling and adsorption mechanism

The sta-phy models are another approach to interpret the adsorption isotherm. Here it was chosen the monolayer model (ML) with one energy site and the double layer (DL) model with one energy site [79,80] (supplementary material **S6**). The DL model showed the best statistical parameters in comparison with the ML (Table S1). Thus, the steric parameters of the adsorption equilibrium of ATZ onto the activated carbon are shown in Fig. 8

The parameter n is the number of molecules per site and is also associated with the anchorage of the molecule on the surface of the adsorbent. When $n > 1$, the molecules tend to be adsorbed in a perpendicular position [81]. If $n \leq 0.5$, the atrazine molecules can be shared by two adsorbent sites (at least), thus reflecting a parallel orientation, and the adsorption is a multi-docking process. If $0.5 < n < 1$, both parallel and inclined orientations are possible.

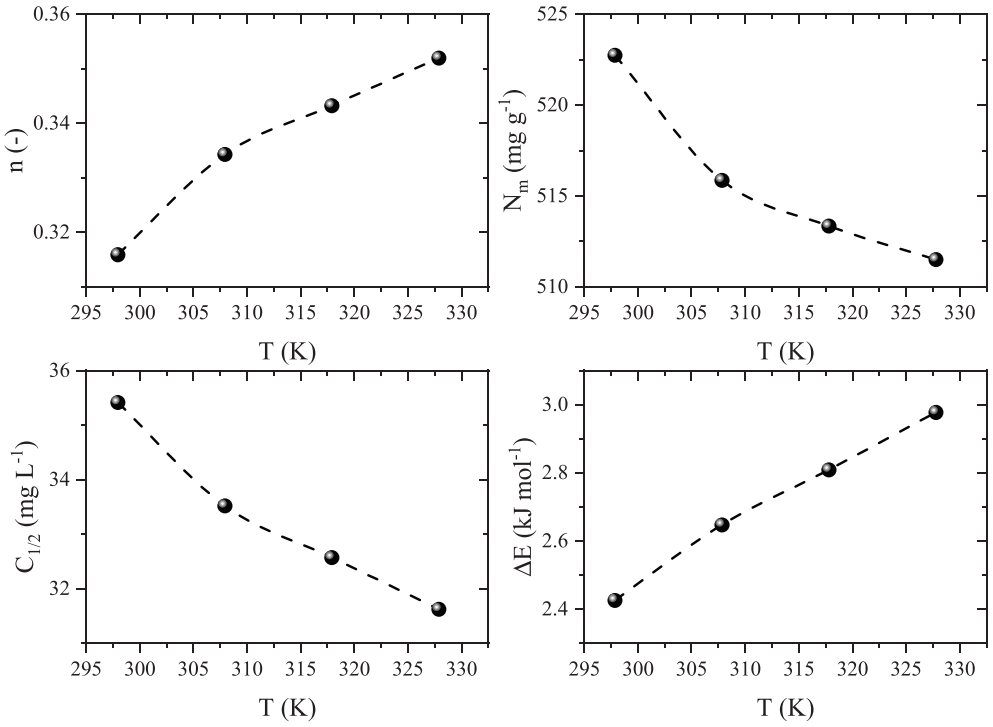

Fig. 8. The behavior of the steric parameters for the double layer model.

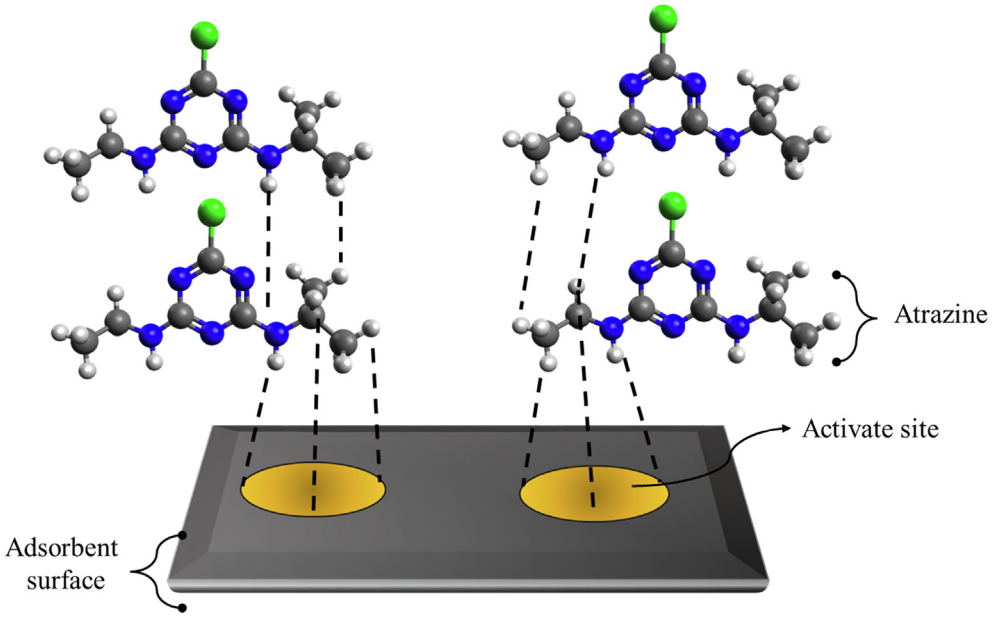

Fig. 9. Schematic demonstration of the ATZ adsorption according to the double layer model.

All n values were lower than 0.5 (Table S1), so the adsorption occurred in Fig. 9. In this case, it was found that n values tend to increase with the temperature. So, the atrazine molecules will be adsorbed parallelly and stacked to each other, forming a double layer due to the hydrogen bonds. The N_m (mg g^{-1}) represents the density of the receptor site, which is related to the adsorption capacity and the number of molecules per site. For his adsorption system, it was found that the N_m tends to decrease with the evolution of the system temperature. This effect is related to the dilatation of the surface due to thermal agitation [82]. The $C_{1/2}$ (mg L^{-1}) is the concentration at half-saturation, which is employed to determine the adsorption energy (ΔE kJ mol^{-1}). For the endothermic adsorption, the $C_{1/2}$ tends to decrease with the temperature. This trend is further corroborated by the adsorption energy, which presented the inverse behavior with the temperature evolution. Furthermore, the adsorption energy was found below 40 kJ mol^{-1}. This trend indicates that the adsorption is a physisorption type [83]. Thus, the adsorption of ATZ onto the activated carbon depends on the hydrogen bonds, electrostatic interactions, and π–π interactions.

3.6. Treatment of the river water sample

A real water sample from the Jacuí river (Agudo, Rio Grande do Sul, Brazil) was collected and treated by adsorption with PSAC. Jacuí is a river surrounded by riparian forests but mainly by extensive crops. It is often used to supply animal drinking fountains; therefore, the analysis and treatment showed that the water resources are highly necessary. The sample presented a 4.7 $\mu g\ L^{-1}$ initial ATZ concentration. However, after the adsorption with PSAC (section 2.7), the remaining ATZ concentration was 0.70 $\mu g\ L^{-1}$. This result represents a removal efficiency of 85%. Besides, the concentration after adsorption with PSAC was below the maximum allowed value of Atrazine in water, considering the Brazilian legislation (2 $\mu g\ L^{-1}$) [7]. Thus PSAC is an efficient adsorbent to treat river waters containing atrazine.

4. Conclusions

Diospyros kaki fruit waste was successfully employed as a precursor material for obtaining high surface area activated carbon, which was highly adsorptive towards atrazine removal in synthetic solutions and river waters. The high adsorption performance of the material is due to its important properties, such as high surface area and pore volume, besides the presence of intrinsic functional groups on the material surface. The isotherm curves were favorable, and the adsorption capacity increased with the temperature in the range from 298 to 328 K. A better fit of the equilibrium curves was found by the Freundlich isotherm model. Thermodynamic studies indicated a spontaneous and endothermic process, where physical forces were responsible for the ATZ adsorption. The kinetic studies found that the equilibrium occurred within 240 min, but most adsorption occurred until 60 min. The experimental data were well represented by the LDF model, obtaining a diffusion coefficient ranging from $0.89x10^{-9}$ to $1.63x10^{-9}$ $cm^2\ s^{-1}$. PSAC adsorbent was also efficient in uptake ATZ from the Jacuí river waters, with a removal percentage of 85%. Therefore, the activated carbon sample prepared from *Diospyros kaki* fruit waste can be employed as a promising adsorbent for treating aqueous systems contaminated with atrazine.

CRediT authorship contribution statement

Yamil L. Salomón: Conceptualization, Investigation, Resources, Writing - original draft. **Jordana Georgin:** Conceptualization, Investigation, Resources. **Dison S. P. Franco:** Methodology. **Matias S. Netto:** Conceptualization. **Daniel G. A. Piccilli:** Conceptualization. **Edson Luiz Foletto:** Conceptualization, Methodology, Formal analysis, Visualization. **Diana Pinto:** Methodology, Formal analysis. **Marcos L. S. Oliveira:** Conceptualization, Methodology, Formal analysis. **Guilherme L. Dotto:** Supervision, Project administration, Funding acquisition, Conceptualization.

Declaration of Competing Interest

The authors declare that they have no known competing financial interests or personal relationships that could have appeared to influence the work reported in this paper.

Appendix A. Supplementary material

Supplementary data to this article can be found online at https://doi.org/10.1016/j.molliq.2021.117990.

References

[1] I. Akpinar, A.O. Yazaydin, Adsorption of Atrazine from Water in Metal-Organic Framework Materials, J. Chem. Eng. Data. 63 (7) (2018) 2368–2375, https://doi.org/10.1021/acs.jced.7b0093010.1021/acs.jced.7b00930.s001.

[2] R. Grillo, A.E.S. Pereira, C.S. Nishisaka, R. De Lima, K. Oehlke, R. Greiner, L.F. Fraceto, Chitosan/tripolyphosphate nanoparticles loaded with paraquat herbicide: An environmentally safer alternative for weed control, J. Hazard. Mater. 278 (2014) 163–171, https://doi.org/10.1016/j.jhazmat.2014.05.079.

[3] V. Kumar, P. Jha, Influence of herbicides applied postharvest in wheat stubble on control, fecundity, and progeny fitness of Kochia scoparia in the US Great Plains, Crop Prot. 71 (2015) 144–149, https://doi.org/10.1016/j.cropro.2015.02.016.

[4] Y. Gao, Z. Jiang, J. Li, W. Xie, Q. Jiang, M. Bi, Y. Zhang, A comparison of the characteristics and atrazine adsorption capacity of co-pyrolysed and mixed biochars generated from corn straw and sawdust, Environ. Res. 172 (2019) 561–568, https://doi.org/10.1016/j.envres.2019.03.010.

[5] P. Vanraes, G. Willems, A. Nikiforov, P. Surmont, F. Lynen, J. Vandamme, J. Van Durme, Y.P. Verheust, S.W.H. Van Hulle, A. Dumoulin, C. Leys, Removal of atrazine in water by combination of activated carbon and dielectric barrier discharge, J. Hazard. Mater. 299 (2015) 647–655, https://doi.org/10.1016/j.jhazmat.2015.07.075.

[6] M. Kica, S. Ronka, The Removal of Atrazine from Water using Specific Polymeric Adsorbent, Sep. Sci. Technol. 49 (11) (2014) 1634–1642, https://doi.org/10.1080/01496395.2014.906461.

[7] S.S. Caldas, J.L.O. Arias, C. Rombaldi, L.L. Mello, M.B.R. Cerqueira, A.F. Martins, E. G. Primel, Occurrence of pesticides and PPCPs in surface and drinking water in southern Brazil: Data on 4-year monitoring, J. Braz. Chem. Soc. 30 (2019) 71–80, https://doi.org/10.21577/0103-5053.20180154.

[8] G.L. Dotto, G. McKay, Current scenario and challenges in adsorption for water treatment, J. Environ. Chem. Eng. 8 (4) (2020) 103988, https://doi.org/10.1016/j.jece:2020.103988.

[9] S. Salvestrini, P. Sagliano, P. Iovino, S. Capasso, C. Colella, Atrazine adsorption by acid-activated zeolite-rich tuffs, Appl. Clay Sci. 49 (3) (2010) 330–335, https://doi.org/10.1016/j.clay.2010.04.008.

[10] X.M. Yan, B.Y. Shi, J.J. Lu, C.H. Feng, D.S. Wang, H.X. Tang, Adsorption and desorption of atrazine on carbon nanotubes, J. Colloid Interface Sci. 321 (1) (2008) 30–38, https://doi.org/10.1016/j.jcis.2008.01.047.

[11] Y. Jia, R. Wang, A.G. Fane, Atrazine adsorption from aqueous solution using powdered activated carbon - Improved mass transfer by air bubbling agitation, Chem. Eng. J. 116 (2006) 53–59, https://doi.org/10.1016/j.cej.2005.10.014.

[12] L. Zhang, L. Sellaoui, D. Franco, G.L. Dotto, A. Bajahzar, H. Belmabrouk, A. Bonilla-Petriciolet, M.L.S. Oliveira, Z. Li, Adsorption of dyes brilliant blue, sunset yellow and tartrazine from aqueous solution on chitosan: Analytical interpretation via multilayer statistical physics model, Chem. Eng. J. 382 (2020) 122952, https://doi.org/10.1016/j.cej.2019.122952.

[13] M.A.M. Salleh, D.K. Mahmoud, W.A.W.A. Karim, A. Idris, Cationic and anionic dye adsorption by agricultural solid wastes: A comprehensive review, Desalination. 280 (1-3) (2011) 1–13, https://doi.org/10.1016/j.desal.2011.07.019.

[14] J. Georgin, F.C. Drumm, P. Grassi, D. Franco, D. Allasia, G.L. Dotto, Potential of Araucaria angustifolia bark as adsorbent to remove Gentian Violet dye from aqueous effluents, Water Sci. Technol. 78 (2018) 1693–1703, https://doi.org/10.2166/wst.2018.448.

[15] S. Hokkanen, A. Bhatnagar, M. Sillanpää, A review on modification methods to cellulose-based adsorbents to improve adsorption capacity, Water Res. 91 (2016) 156–173, https://doi.org/10.1016/j.watres.2016.01.008.

[16] N. Eibisch, R. Schroll, R. Fuß, R. Mikutta, M. Helfrich, H. Flessa, Pyrochars and hydrochars differently alter the sorption of the herbicide isoproturon in an agricultural soil, Chemosphere. 119 (2015) 155–162, https://doi.org/10.1016/j.chemosphere.2014.05.059.

[17] Y.J. Liu, C.Y. Hu, S.L. Lo, Direct and indirect electrochemical oxidation of amine-containing pharmaceuticals using graphite electrodes, J. Hazard. Mater. 366 (2019) 592–605, https://doi.org/10.1016/j.jhazmat.2018.12.037.

[18] X. Wei, Z. Wu, Z. Wu, B.C. Ye, Adsorption behaviors of atrazine and Cr(III) onto different activated carbons in single and co-solute systems, Powder Technol. 329 (2018) 207–216, https://doi.org/10.1016/j.powtec.2018.01.060.

[19] E. Tchikuala, P. Mourão, J. Nabais, Valorisation of Natural Fibres from African Baobab Wastes by the Production of Activated Carbons for Adsorption of Diuron, Procedia Eng. 200 (2017) 399–407, https://doi.org/10.1016/j.proeng.2017.07.056.

[20] Y.L.d.O. Salomón, J. Georgin, D.S.P. Franco, M.S. Netto, D.G.A. Piccilli, E.L. Foletto, L.F.S. Oliveira, G.L. Dotto, High-performance removal of 2,4-dichlorophenoxyacetic acid herbicide in water using activated carbon derived from Queen palm fruit endocarp (Syagrus romanzoffiana), J. Environ. Chem. Eng. 9 (1) (2021) 104911, https://doi.org/10.1016/j.jece:2020.104911.

[21] Q.A. Binh, H.-H. Nguyen, Investigation the isotherm and kinetics of adsorption mechanism of herbicide 2,4-dichlorophenoxyacetic acid (2,4-D) on corn cob biochar, Bioresour. Technol. Reports. 11 (2020) 100520, https://doi.org/10.1016/j.biteb.2020.100520.

[22] C. Guan, P. Zhang, M. Wu, M. Zeng, S. Chachar, X. Ruan, R. Wang, Y. Yang, Discovery of a millennial androecious germplasm and its potential in persimmon (Diospyros kaki Thunb.) breeding, Sci. Hortic. (Amsterdam). 269 (2020) 109392, https://doi.org/10.1016/j.scienta.2020.109392.

[23] H. Ko, G. Huh, S.H. Jung, H. Kwon, Y. Jeon, Y.N. Park, Y.-J. Kim, Diospyros kaki leaves inhibit HGF/Met signaling-mediated EMT and stemness features in hepatocellular carcinoma, Food Chem. Toxicol. 142 (2020) 111475, https://doi.org/10.1016/j.fct.2020.111475.
[24] Y. Zhang, L. Zhao, S.W. Huang, W. Wang, S.J. Song, Triterpene saponins with neuroprotective effects from the leaves of Diospyros kaki Thunb, Fitoterapia. 129 (2018) 138–144, https://doi.org/10.1016/j.fitote.2018.06.023.
[25] M.P. Cano, A. Gómez-Maqueo, R. Fernández-López, J. Welti-Chanes, T. García-Cayuela, Impact of high hydrostatic pressure and thermal treatment on the stability and bioaccessibility of carotenoid and carotenoid esters in astringent persimmon (Diospyros kaki Thunb, var. Rojo Brillante), Food Res. Int. 123 (2019) 538–549, https://doi.org/10.1016/j.foodres.2019.05.017.
[26] C. Ancillotti, S. Orlandini, L. Ciofi, B. Pasquini, C. Caprini, C. Droandi, S. Furlanetto, M. Del Bubba, Quality by design compliant strategy for the development of a liquid chromatography–tandem mass spectrometry method for the determination of selected polyphenols in Diospyros kaki, J. Chromatogr. A. 1569 (2018) 79–90, https://doi.org/10.1016/j.chroma.2018.07.046.
[27] H. Freundlich, Über die Adsorption in Lösungen, Zeitschrift Für Phys. Chemie. 57U (1907). https://doi.org/10.1515/zpch-1907-5723.
[28] M.M. Dubinin, V.A. Astakhov, Development of the concepts of volume filling of micropores in the adsorption of gases and vapors by microporous adsorbents, Bull. Acad. Sci. USSR Div. Chem. Sci. 20 (1) (1971) 3–7, https://doi.org/10.1007/BF00849307.
[29] M. Temkin, V. Pyzhev, Kinetics of the synthesis of ammonia on promoted iron catalysts, Jour. Phys. Chem. (U.S.S.R.). 13 (1939) 851–867.
[30] I. Langmuir, The adsorption of gases on plane surfaces of glass, mica and platinum, J. Am. Chem. Soc. 40 (9) (1918) 1361–1403, https://doi.org/10.1021/ja02242a004.
[31] E.C. Lima, A. Hosseini-Bandegharaei, J.C. Moreno-Piraján, I. Anastopoulos, A critical review of the estimation of the thermodynamic parameters on adsorption equilibria. Wrong use of equilibrium constant in the Van't Hoof equation for calculation of thermodynamic parameters of adsorption, J. Mol. Liq. 273 (2019) 425–434, https://doi.org/10.1016/j.molliq.2018.10.048.
[32] E. Glueckauf, Theory of chromatography. Part 10.—Formulæ for diffusion into spheres and their application to chromatography, Trans. Faraday Soc. 51 (0) (1955) 1540–1551, https://doi.org/10.1039/TF9555101540.
[33] M. Thommes, K. Kaneko, A.V. Neimark, J.P. Olivier, F. Rodriguez-Reinoso, J. Rouquerol, K.S.W. Sing, Physisorption of gases, with special reference to the evaluation of surface area and pore size distribution (IUPAC Technical Report), Pure Appl. Chem. 87 (2015) 1051–1069, https://doi.org/10.1515/pac-2014-1117.
[34] D.R. Lima, A. Hosseini-Bandegharaei, P.S. Thue, E.C. Lima, Y.R.T. de Albuquerque, G.S. dos Reis, C.S. Umpierres, S.L.P. Dias, H.N. Tran, Efficient acetaminophen removal from water and hospital effluents treatment by activated carbons derived from Brazil nutshells, Colloids Surfaces A Physicochem. Eng. Asp. 583 (2019) 123966, https://doi.org/10.1016/j.colsurfa.2019.123966.
[35] F.M. Kasperiski, E.C. Lima, C.S. Umpierres, G.S. dos Reis, P.S. Thue, D.R. Lima, S.L. P. Dias, C. Saucier, J.B. da Costa, Production of porous activated carbons from Caesalpinia ferrea seed pod wastes: Highly efficient removal of captopril from aqueous solutions, J. Clean. Prod. 197 (2018) 919–929, https://doi.org/10.1016/j.jclepro.2018.06.146.
[36] A.B. Leite, C. Saucier, E.C. Lima, G.S. dos Reis, C.S. Umpierres, B.L. Mello, M. Shirmardi, S.L.P. Dias, C.H. Sampaio, Activated carbons from avocado seed: optimisation and application for removal of several emerging organic compounds, Environ. Sci. Pollut. Res. 25 (8) (2018) 7647–7661, https://doi.org/10.1007/s11356-017-1105-9.
[37] J. Georgin, D. Franco, F.C.F.C. Drumm, P. Grassi, M.S.M.S. Netto, D. Allasia, G.L.G. L. Dotto, Powdered biosorbent from the mandacaru cactus (cereus jamacaru) for discontinuous and continuous removal of Basic Fuchsin from aqueous solutions, Powder Technol. 364 (2020) 584–592, https://doi.org/10.1016/j.powtec.2020.01.064.
[38] J. Georgin, Y.L. de O. Salomón, D.S.P. Franco, M.S. Netto, D.G.A. Piccilli, E.L. Foletto, G.L. Dotto, Successful adsorption of bright blue and methylene blue on modified pods of Caesalpinia echinata in discontinuous system, Environ. Sci. Pollut. Res. 28 (7) (2021) 8407–8420, https://doi.org/10.1007/s11356-020-11210-3.
[39] Y.L. de O. Salomón, J. Georgin, G.S. dos Reis, É.C. Lima, M.L.S. Oliveira, D.S.P. Franco, M.S. Netto, D. Allasia, G.L. Dotto, Utilization of Pacara Earpod tree (Enterolobium contortisilquum) and Ironwood (Caesalpinia leiostachya) seeds as low-cost biosorbents for removal of basic fuchsin, Environ. Sci. Pollut. Res. 27 (26) (2020) 33307–33320, https://doi.org/10.1007/s11356-020-09471-z.
[40] A. Medhat, H.H. El-Maghrabi, A. Abdelghany, N.M. Abdel Menem, P. Raynaud, Y.M. Moustafa, M.A. Elsayed, A.A. Nada, Efficiently activated carbons from corn cob for methylene blue adsorption, Appl. Surf. Sci. Adv. 3 (2021) 100037, https://doi.org/10.1016/j.apsadv.2020.100037.
[41] M. Bounaas, A. Bouguettoucha, D. Chebli, J.M. Gatica, H. Vidal, Role of the Wild Carob as Biosorbent and as Precursor of a New High-Surface-Area Activated Carbon for the Adsorption of Methylene Blue, Arab. J. Sci. Eng. 46 (1) (2021) 325–341, https://doi.org/10.1007/s13369-020-04739-5.
[42] H.N. Tran, S.J. You, H.P. Chao, Fast and efficient adsorption of methylene green 5 on activated carbon prepared from new chemical activation method, J. Environ. Manage. 188 (2017) 322–336, https://doi.org/10.1016/j.jenvman.2016.12.003.
[43] N.L.I. Zailuddin, S. Husseinsyah, F.N. Hahary, H. Ismail, Treatment of oil palm empty fruit bunch regenerated cellulose biocomposite films using methacrylic acid, BioResources. 11 (2016) 873–885. https://doi.org/10.15376/biores.11.1.873-885.
[44] X. Zhu, Y. Liu, C. Zhou, G. Luo, S. Zhang, J. Chen, A novel porous carbon derived from hydrothermal carbon for efficient adsorption of tetracycline, Carbon N. Y. 77 (2014) 627–636, https://doi.org/10.1016/j.carbon.2014.05.067.
[45] K. Le Van, T.T. Luong Thi, Activated carbon derived from rice husk by NaOH activation and its application in supercapacitor, Prog. Nat. Sci. Mater. Int. 24 (3) (2014) 191–198, https://doi.org/10.1016/j.pnsc.2014.05.012.
[46] J. Georgin, G.L. Dotto, M.A. Mazutti, E.L. Foletto, Preparation of activated carbon from peanut shell by conventional pyrolysis and microwave irradiation-pyrolysis to remove organic dyes from aqueous solutions, J. Environ. Chem. Eng. 4 (1) (2016) 266–275, https://doi.org/10.1016/j.jece:2015.11.018.
[47] M.A. Ahmad, N.A. Ahmad Puad, O.S. Bello, Kinetic, equilibrium and thermodynamic studies of synthetic dye removal using pomegranate peel activated carbon prepared by microwave-induced KOH activation, Water Resour, Ind. 6 (2014) 18–35, https://doi.org/10.1016/j.wri.2014.06.002.
[48] M.A. Zazycki, M. Godinho, D. Perondi, E.L. Foletto, G.C. Collazzo, G.L. Dotto, New biochar from pecan nutshells as an alternative adsorbent for removing reactive red 141 from aqueous solutions, J. Clean. Prod. 171 (2018) 57–65, https://doi.org/10.1016/j.jclepro.2017.10.007.
[49] L.M. Ndjientcheu Yossa, S.K. Ouiminga, S.S. Sidibe, I.W.K. Ouedraogo, Synthesis of a cleaner potassium hydroxide-activated carbon from baobab seeds hulls and investigation of adsorption mechanisms for diuron, Sci. African. 9 (2020) e00476, https://doi.org/10.1016/j.sciaf.2020.e00476.
[50] Z. Xie, W. Guan, F. Ji, Z. Song, Y. Zhao, Production of biologically activated carbon from orange peel and landfill leachate subsequent treatment technology, J. Chem. 2014 (2014) 1–9, https://doi.org/10.1155/2014/491912.
[51] Y. Cui, A. Masud, N. Aich, J.D. Atkinson, Phenol and Cr(VI) removal using materials derived from harmful algal bloom biomass: Characterization and performance assessment for a biosorbent, a porous carbon, and Fe/C composites, J. Hazard. Mater. 368 (2019) 477–486, https://doi.org/10.1016/j.jhazmat.2019.01.075.
[52] A.C. Lua, T. Yang, J. Guo, Effects of pyrolysis conditions on the properties of activated carbons prepared from pistachio-nut shells, J. Anal. Appl. Pyrolysis. 72 (2) (2004) 279–287, https://doi.org/10.1016/j.jaap.2004.08.001.
[53] G.F. De Oliveira, R.C. De Andrade, M.A.G. Trindade, H.M.C. Andrade, C.T. De Carvalho, Thermogravimetric and spectroscopic study (Tg-DTA/FT-IR) of activated carbon from the renewable biomass source babassu, Quim. Nova. 40 (2017) 284–292. https://doi.org/10.21577/0100-4042.20160191.
[54] S.F. Lütke, A.V. Igansi, L. Pegoraro, G.L. Dotto, L.A.A. Pinto, T.R.S. Cadaval, Preparation of activated carbon from black wattle bark waste and its application for phenol adsorption, J. Environ. Chem. Eng. 7 (5) (2019) 103396, https://doi.org/10.1016/j.jece:2019.103396.
[55] N.K. Niazi, I. Bibi, M. Shahid, Y.S. Ok, S.M. Shaheen, J. Rinklebe, H. Wang, B. Murtaza, E. Islam, M. Farrakh Nawaz, A. Lüttge, Arsenic removal by Japanese oak wood biochar in aqueous solutions and well water: Investigating arsenic fate using integrated spectroscopic and microscopic techniques, Sci. Total Environ. 621 (2018) 1642–1651, https://doi.org/10.1016/j.scitotenv.2017.10.063.
[56] H.B. Quesada, T.P. de Araújo, L.F. Cusioli, M.A.S.D. de Barros, R.G. Gomes, R. Bergamasco, Evaluation of novel activated carbons from chichá-do-cerrado (Sterculia striata St. Hil. et Naud) fruit shells on metformin adsorption and treatment of a synthetic mixture, J. Environ Chem. Eng. 9 (1) (2021) 104914, https://doi.org/10.1016/j.jece:2020.104914.
[57] Y. Wang, S.-L. Wang, T. Xie, J. Cao, Activated carbon derived from waste tangerine seed for the high-performance adsorption of carbamate pesticides from water and plant, Bioresour. Technol. 316 (2020) 123929, https://doi.org/10.1016/j.biortech.2020.123929.
[58] A. Bonilla-Petriciolet, D.I. Mendoza-Castillo, H.E. Reynel-Avila, Adsorption Processes for Water Treatment and Purification, Springer International Publishing, Cham (2017), https://doi.org/10.1007/978-3-319-58136-1.
[59] G. Moussavi, R. Khosravi, The removal of cationic dyes from aqueous solutions by adsorption onto pistachio hull waste, Chem. Eng. Res. Des. 89 (10) (2011) 2182–2189, https://doi.org/10.1016/j.cherd.2010.11.024.
[60] A. Alahabadi, G. Moussavi, Preparation, characterization and atrazine adsorption potential of mesoporous carbonate-induced activated biochar (CAB) from Calligonum Comosum biomass: Parametric experiments and kinetics, equilibrium and thermodynamic modeling, J. Mol. Liq. 242 (2017) 40–52, https://doi.org/10.1016/j.molliq.2017.06.116.
[61] P. Chingombe, B. Saha, R.J. Wakeman, Sorption of atrazine on conventional and surface modified activated carbons, J. Colloid Interface Sci. 302 (2) (2006) 408–416, https://doi.org/10.1016/j.jcis.2006.06.065.
[62] N.W. Brown, E.P.L. Roberts, A. Chasiotis, T. Cherdron, N. Sanghrajka, Atrazine removal using adsorption and electrochemical regeneration, Water Res. 38 (13) (2004) 3067–3074, https://doi.org/10.1016/j.watres.2004.04.043.
[63] I.D. Kovaios, C.A. Paraskeva, P.G. Koutsoukos, Adsorption of atrazine from aqueous electrolyte solutions on humic acid and silica, J. Colloid Interface Sci. 356 (1) (2011) 277–285, https://doi.org/10.1016/j.jcis.2011.01.002.
[64] D.L.D. Lima, C.P. Silva, R.J. Schneider, V.I. Esteves, Development of an ELISA procedure to study sorption of atrazine onto a sewage sludge-amended luvisol soil, Talanta. 85 (3) (2011) 1494–1499, https://doi.org/10.1016/j.talanta.2011.06.024.
[65] J. Li, Y. Li, J. Lu, Adsorption of herbicides 2,4-D and acetochlor on inorganic-organic bentonites, Appl. Clay Sci. 46 (3) (2009) 314–318, https://doi.org/10.1016/j.clay.2009.08.032.

[66] Y. Tang, S. Luo, Y. Teng, C. Liu, X. Xu, X. Zhang, L. Chen, Efficient removal of herbicide 2,4-dichlorophenoxyacetic acid from water using Ag/reduced graphene oxide co-decorated TiO2 nanotube arrays, J. Hazard. Mater. 241–242 (2012) 323–330, https://doi.org/10.1016/j.jhazmat.2012.09.050.
[67] J. Lladó, C. Lao-Luque, B. Ruiz, E. Fuente, M. Solé-Sardans, A.D. Dorado, Role of activated carbon properties in atrazine and paracetamol adsorption equilibrium and kinetics, Process Saf. Environ. Prot. 95 (2015) 51–59, https://doi.org/10.1016/j.psep.2015.02.013.
[68] L. Yue, C.J. Ge, D. Feng, H. Yu, H. Deng, B. Fu, Adsorption–desorption behavior of atrazine on agricultural soils in China, J. Environ. Sci. (China) 57 (2017) 180–189, https://doi.org/10.1016/j.jes.2016.11.002.
[69] X. Wei, Z. Wu, C. Du, Z. Wu, B.C. Ye, G. Cravotto, Enhanced adsorption of atrazine on a coal-based activated carbon modified with sodium dodecyl benzene sulfonate under microwave heating, J. Taiwan Inst. Chem. Eng. 77 (2017) 257–262, https://doi.org/10.1016/j.jtice.2017.04.004.
[70] Y. Zhang, B. Cao, L. Zhao, L. Sun, Y. Gao, J. Li, F. Yang, Biochar-supported reduced graphene oxide composite for adsorption and coadsorption of atrazine and lead ions, Appl. Surf. Sci. 427 (2018) 147–155, https://doi.org/10.1016/j.apsusc.2017.07.237.
[71] B. Chen, Z. Chen, Sorption of naphthalene and 1-naphthol by biochars of orange peels with different pyrolytic temperatures, Chemosphere. 76 (1) (2009) 127–133, https://doi.org/10.1016/j.chemosphere.2009.02.004.
[72] X. Zhao, J. Chen, F. Chen, X. Wang, Q. Zhu, Q. Ao, Surface characterization of corn stalk superfine powder studied by FTIR and XRD, Colloids Surfaces B Biointerfaces. 104 (2013) 207–212, https://doi.org/10.1016/j.colsurfb.2012.12.003.
[73] H.P. Toledo-Jaldin, A. Blanco-Flores, V. Sánchez-Mendieta, O. Martín-Hernández, Influence of the chain length of surfactant in the modification of zeolites and clays. Removal of atrazine from water solutions, Environ. Technol. (United Kingdom). 39 (20) (2018) 2679–2690, https://doi.org/10.1080/09593330.2017.1365097.
[74] Y. Tao, S. Hu, S. Han, H. Shi, Y. Yang, H. Li, Y. Jiao, Q. Zhang, M.S. Akindolie, M. Ji, Z. Chen, Y. Zhang, Efficient removal of atrazine by iron-modified biochar loaded Acinetobacter lwoffii DNS32, Sci. Total Environ. 682 (2019) 59–69, https://doi.org/10.1016/j.scitotenv.2019.05.134.
[75] F.M. Machado, C.P. Bergmann, T.H.M. Fernandes, E.C. Lima, B. Royer, T. Calvete, S.B. Fagan, Adsorption of Reactive Red M-2BE dye from water solutions by multi-walled carbon nanotubes and activated carbon, J. Hazard. Mater. 192 (3) (2011) 1122–1131, https://doi.org/10.1016/j.jhazmat.2011.06.020.
[76] M. Vithanage, S.S. Mayakaduwa, I. Herath, Y.S. Ok, D. Mohan, Kinetics, thermodynamics and mechanistic studies of carbofuran removal using biochars from tea waste and rice husks, Chemosphere. 150 (2016) 781–789, https://doi.org/10.1016/j.chemosphere.2015.11.002.
[77] A. Zuorro, G. Maffei, R. Lavecchia, Kinetic modeling of azo dye adsorption on non-living cells of Nannochloropsis oceanica, J. Environ. Chem. Eng. 5 (4) (2017) 4121–4127, https://doi.org/10.1016/j.jece:2017.07.078.
[78] J. Moreno-Pérez, P.S. Pauletto, A.M. Cunha, Á. Bonilla-Petriciolet, N.P.G. Salau, G.L. Dotto, Three-dimensional mass transport modeling of pharmaceuticals adsorption inside ZnAl/biochar composite, Colloids Surfaces A Physicochem. Eng. Asp. 614 (2021) 126170, https://doi.org/10.1016/j.colsurfa.2021.126170.
[79] X. Pang, L. Sellaoui, D. Franco, M.S. Netto, J. Georgin, G. Luiz Dotto, M.K. Abu Shayeb, H. Belmabrouk, A. Bonilla-Petriciolet, Z. Li, Preparation and characterization of a novel mountain soursop seeds powder adsorbent and its application for the removal of crystal violet and methylene blue from aqueous solutions, Chem. Eng. J. 391 (2020) 123617, https://doi.org/10.1016/j.cej.2019.123617.
[80] X. Pang, L. Sellaoui, D. Franco, G.L. Dotto, J. Georgin, A. Bajahzar, H. Belmabrouk, A. Ben Lamine, A. Bonilla-Petriciolet, Z. Li, Adsorption of crystal violet on biomasses from pecan nutshell, para chestnut husk, araucaria bark and palm cactus: Experimental study and theoretical modeling via monolayer and double layer statistical physics models, Chem. Eng. J. 378 (2019) 122101, https://doi.org/10.1016/j.cej.2019.122101.
[81] L. Sellaoui, H. Guedidi, S. Knani, L. Reinert, L. Duclaux, A.B. Lamine, Application of statistical physics formalism to the modeling of adsorption isotherms of ibuprofen on activated carbon, Fluid phase Equilib. 387 (2015) 103–110, https://doi.org/10.1016/j.fluid.2014.12.018.
[82] A. Nakbi, M. Bouzid, F. Ayachi, F. Aouaini, A. Ben Lamine, Investigation of caffeine taste mechanism through a statistical physics modeling of caffeine dose-taste response curve by a biological putative caffeine adsorption process in electrophysiological response, Prog. Biophys. Mol. Biol. 149 (2019) 70–85, https://doi.org/10.1016/j.pbiomolbio.2018.12.013.
[83] A. Nakbi, M. Bouzid, F. Ayachi, N. Bouaziz, A. Ben Lamine, Quantitative characterization of sucrose taste by statistical physics modeling parameters using an analogy between an experimental physicochemical isotherm of sucrose adsorption on β-cyclodextrin and a putative biological sucrose adsorption from sucrose d, J. Mol. Liq. 298 (2020), https://doi.org/10.1016/j.molliq.2019.111950 111950.